nature genetics

Recurrent activating *ACVR1* mutations in diffuse intrinsic pontine glioma

Kathryn R Taylor[1,13], Alan Mackay[1,13], Nathalène Truffaux[2], Yaron S Butterfield[3], Olena Morozova[4], Cathy Philippe[2], David Castel[2], Catherine S Grasso[5], Maria Vinci[1], Diana Carvalho[1], Angel M Carcaboso[6], Carmen de Torres[6], Ofelia Cruz[6], Jaume Mora[6], Natacha Entz-Werle[7], Wendy J Ingram[8], Michelle Monje[9], Darren Hargrave[10], Alex N Bullock[11], Stéphanie Puget[12], Stephen Yip[3], Chris Jones[1] & Jacques Grill[2]

Diffuse intrinsic pontine gliomas (DIPGs) are highly infiltrative malignant glial neoplasms of the ventral pons that, due to their location within the brain, are unsuitable for surgical resection and consequently have a universally dismal clinical outcome. The median survival time is 9–12 months, with neither chemotherapeutic nor targeted agents showing substantial survival benefit in clinical trials in children with these tumors[1]. We report the identification of recurrent activating mutations in the *ACVR1* gene, which encodes a type I activin receptor serine/threonine kinase, in 21% of DIPG samples. Strikingly, these somatic mutations (encoding p.Arg206His, p.Arg258Gly, p.Gly328Glu, p.Gly328Val, p.Gly328Trp and p.Gly356Asp substitutions) have not been reported previously in cancer but are identical to mutations found in the germ line of individuals with the congenital childhood developmental disorder fibrodysplasia ossificans progressiva (FOP)[2] and have been shown to constitutively activate the BMP–TGF-β signaling pathway. These mutations represent new targets for therapeutic intervention in this otherwise incurable disease.

Recent high-throughput sequencing approaches have found a striking prevalence of mutations in the genes for the histone variants H3.3 (*H3F3A*) or H3.1 (*HIST1H3B*) that encode p.Lys27Met substitutions in the childhood brain tumor DIPG[3]. This lysine-to-methionine substitution confers a *trans*-dominant ablation of global trimethylation at lysine 27 of histone H3 (H3K27me3), which likely profoundly alters gene expression through the derepression of Polycomb repressive complex 2 (PRC2) target genes[4]. Despite these advances in understanding of the distinct biology of these tumors[1], approaches for desperately needed specific therapeutic interventions are not clear, and little has been reported of the additional mutations accompanying these changes.

We carried out whole-genome sequencing on a unique series of 20 pretreatment biopsy samples of DIPG, for which the patients underwent a safe stereotactic procedure[5], and whole-exome sequencing on a further biopsy case as well as 5 samples obtained at autopsy (**Supplementary Table 1**). Histone H3 gene mutations encoding p.Lys27Met were observed in 23 of 26 cases (88%), comprising 15 (58%) *H3F3A* mutations and 8 (31%) *HIST1H3B* mutations (**Fig. 1a**). These were not found in concert with mutations in the chaperones *ATRX* or *DAXX* as has been described for supratentorial pediatric glioblastoma (pGBM)[6]. There was also an absence of other known glioma-related molecular abnormalities such as *IDH1*, *IDH2*, *BRAF* or *FGFR1* mutations and gene fusions. The mutational spectrum of the untreated biopsy cases was not significantly different from that of the autopsy cases ($P > 0.05$; **Fig. 1b**), although the treatment-naive samples had a low overall mutation rate, with a mean of 14.8 somatic single-nucleotide variants (SNVs) per sample (range of 0–25), that was significantly lower than observed in the radiation-treated autopsy cases (mean = 32.0, range = 14–50; $P = 0.004$, *t* test). Similarly, there was a significantly lower overall mutation rate in untreated samples taken at biopsy than in autopsy samples (mean of 0.76 versus 1.2 mutations per megabase; $P = 0.023$, *t* test).

Eleven of 26 DIPGs (42%) harbored somatic *TP53* mutations, with a further 6 cases (23%) shown to have SNVs in *PPM1D*, which encodes a regulator of p38 mitogen-activated protein kinase (p38-MAPK)-p53 signaling in response to cellular stress, and an additional case with a somatic *ATM* mutation (**Supplementary Fig. 1**), demonstrating non-overlapping targeting of a DNA damage response pathway in 18 of 26 DIPGs (69%) (**Supplementary Fig. 2**). We further identified non-overlapping recurrent alterations in the phosphoinositide 3-kinase (PI3K) pathway targeting *PIK3CA*, *PIK3R1* and *PTEN* through SNVs and microdeletion (**Supplementary Fig. 3**), in addition to amplification of *MET* (1/26; 4%) as previously described[7,8] and truncating

[1]Institute of Cancer Research, London, UK. [2]CNRS UMR 8203, Gustave Roussy, University Paris Sud, Villejuif, France. [3]BC Cancer Agency, Vancouver, British Columbia, Canada. [4]Biomolecular Engineering, University of California, Santa Cruz, Santa Cruz, California, USA. [5]Department of Molecular and Medical Genetics, Oregon Health and Science University, Portland, Oregon, USA. [6]Pediatric Hematology and Oncology, Hospital Sant Joan de Déu, Barcelona, Spain. [7]Centre Hospitalier Regional et Universitaire Hautepierre, Strasbourg, France. [8]Queensland Children's Tumour Bank, Queensland Children's Medical Research Institute, The University of Queensland, Brisbane, Queensland, Australia. [9]Stanford Institute for Stem Cell Biology and Regenerative Medicine, Stanford University School of Medicine, Stanford, California, USA. [10]Neuro-oncology and Experimental Therapeutics, Great Ormond Street Hospital, London, UK. [11]Structural Genomics Consortium, University of Oxford, Oxford, UK. [12]Pediatric Neurosurgery, Necker Sick Children's Hospital, Paris, France. [13]These authors contributed equally to this work. Correspondence should be addressed to C.J. (chris.jones@icr.ac.uk) or J.G. (grill@igr.fr).

Received 30 April 2013; accepted 21 February 2014; published online 6 April 2014; doi:10.1038/ng.2925

mutation of *NF1* (1/26; 4%) (**Fig. 1c**). We also identified new recurrent somatic mutations in *IGF2R* (2/26; 8%), although these mutations were concurrent with others in the pathway, such that their consequences are unknown. In total, 12 of 26 DIPG cases (46%) harbored some form of alteration predicted to activate the receptor tyrosine kinase (RTK)-PI3K-MAPK pathways (**Supplementary Fig. 4**).

Heterozygous somatic coding mutations in the *ACVR1* gene, which encodes the activin A type I receptor ALK2, were observed in 7 of 26 cases (27%) (**Fig. 1c**). These were restricted specifically to codons 328 (c.983G>T, p.Gly328Val, two cases; c.983G>A, p.Gly328Glu, two cases), 258 (c.772C>T, p.Arg258Gly, one case) and 356 (c.1067G>A, p.Gly356Asp, one case), all within the serine/threonine kinase domain, and 206 (c.617G>A, p.Arg206His, one case), within the glycine-serine-rich (GS) domain. Screening an extended series of 26 DIPG biopsy samples by Sanger sequencing identified further recurrences of these mutations and an additional variant at

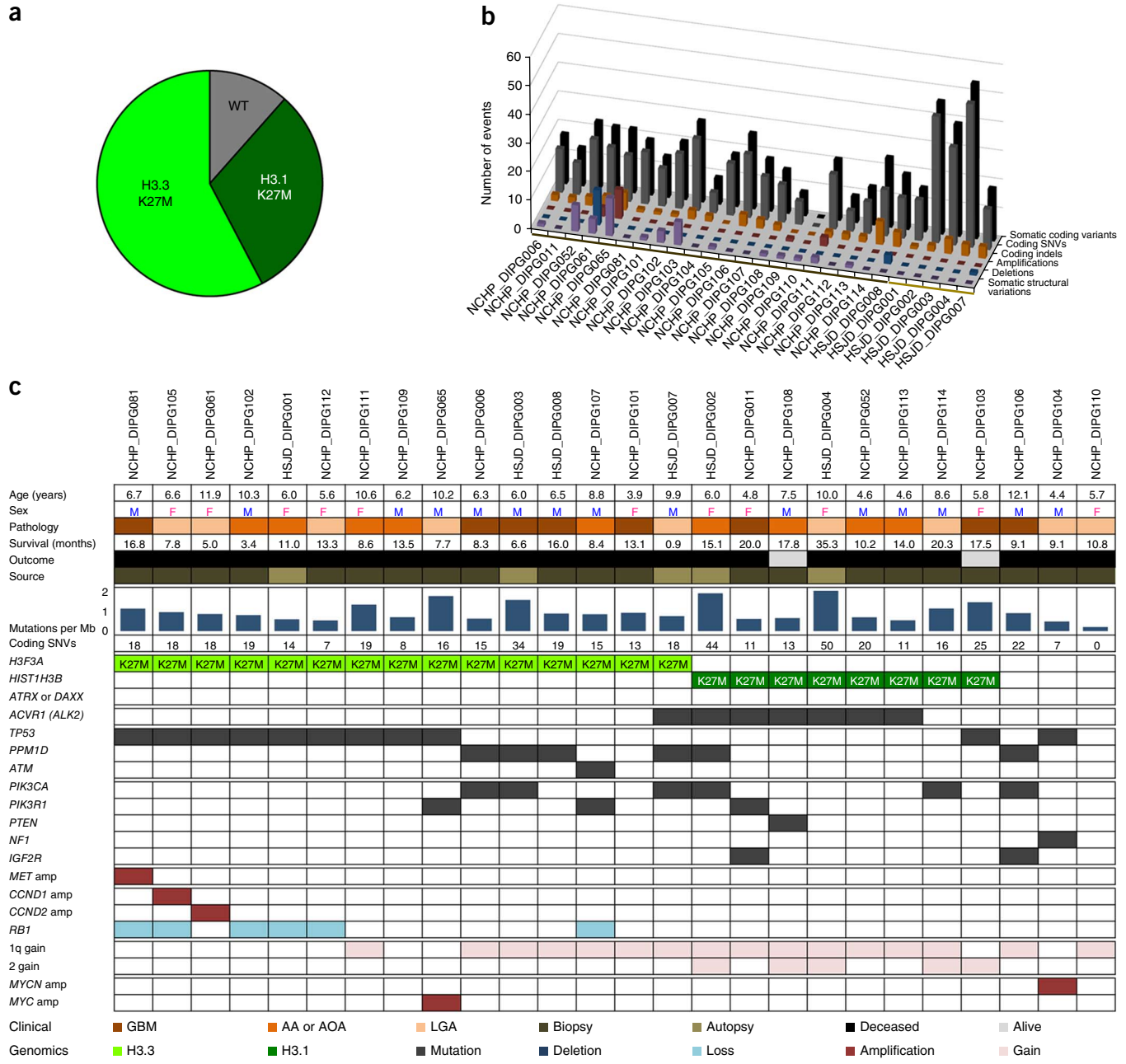

Figure 1 Genomic landscape of DIPG. (**a**) Pie chart showing the breakdown of histone H3 mutations in our series of 26 DIPG samples (*H3F3A* mutation encoding p.Lys27Met: 15/26, 58%; *HIST1H3B* mutation encoding p.Lys27Met: 8/26, 31%, wild-type histone H3: 3/26, 11%). (**b**) Mutational spectrum of DIPG. Bar chart showing the total number of somatic coding variants, coding SNVs, indels, amplifications, deletions and structural variations for each DIPG case. Biopsy cases are marked by the dark brown bar along the *x* axis, and autopsy cases are marked by the light brown bar. (**c**) Summary of major alterations found. Clinicopathological information for the 26 DIPG samples is provided along with the mutation rate and number of somatic coding SNVs. Mutations, amplifications and deletions are noted for the histone H3 genes and *ATRX* or *DAXX*, *ACVR1*, the *ATM-TP53-PPM1D* axis, members of the PI3K-MAPK signaling pathways, RTKs and members of the RB pathway as are chromosome 1q and 2 single-copy gains and amplification (amp) of *MYC* or *MYCN*. GBM, glioblastoma multiforme; AA, anaplastic astrocytoma; AOA, anaplastic oligoastrocytoma; LGA, low-grade astrocytoma; M, male; F, female.

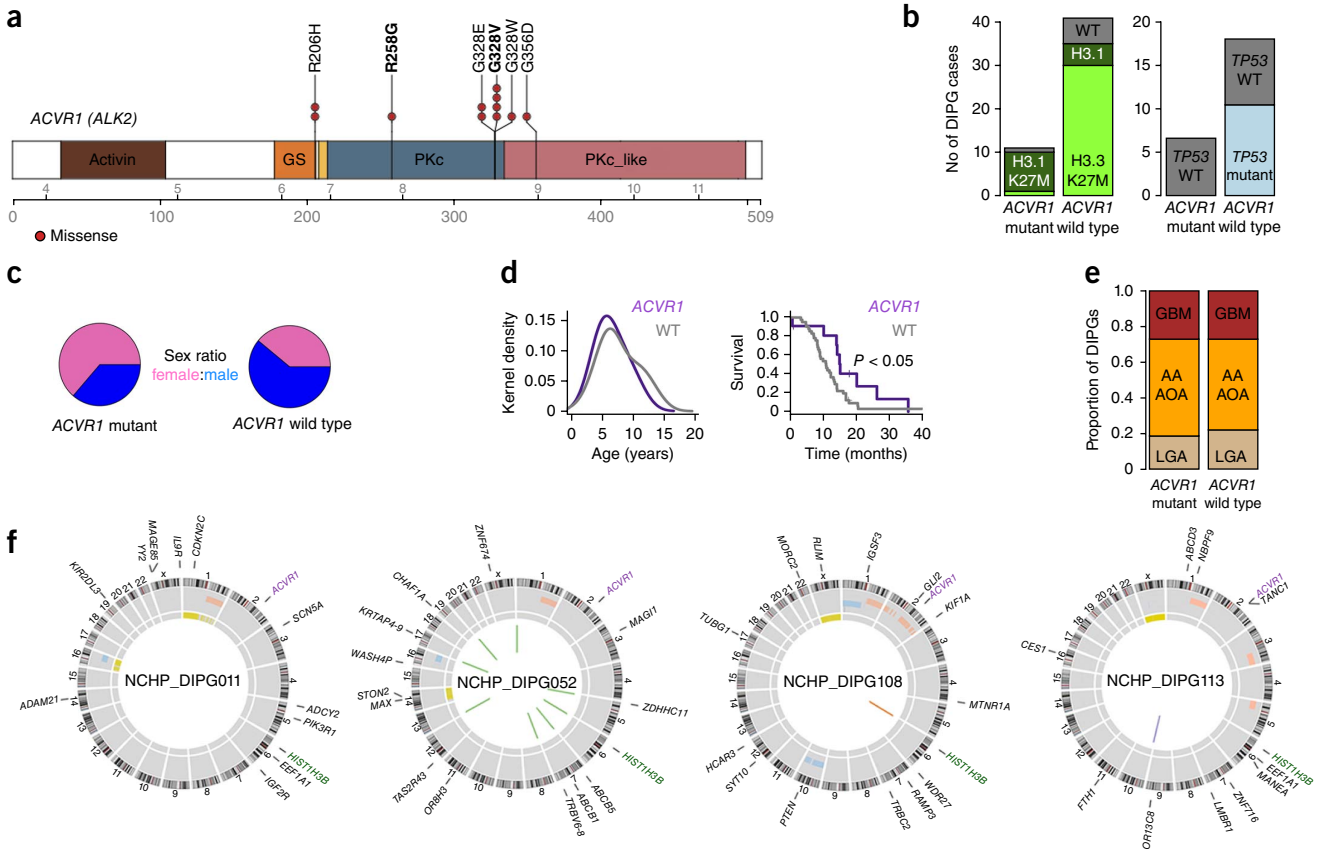

Figure 2 Recurrent *ACVR1* mutations in DIPG. (**a**) Schematic showing recurrent missense mutations in *ACVR1*, overlaid with functional protein domains and exon boundaries. In total, 11 of 52 DIPGs (21%) harbored somatic alterations at 4 residues, all of which have previously been described in the germ line of individuals with FOP. Specific base changes that may be unique to DIPG are highlighted in bold. Activin, activin type I and II receptor domain; GS, TGF-β glycine-serine-rich domain; PKc, protein kinase catalytic domain; PKc_like, protein kinase catalytic domain like. (**b**) Bar graphs showing segregation of activating mutations in *ACVR1* with *HIST1H3B* mutations encoding p.Lys27Met ($P < 0.0001$, Fisher's exact test) and with wild-type (WT) *TP53* ($P = 0.0103$, Fisher's exact test) in our extended series of 52 DIPG cases. (**c**) Sex distribution of cases with *ACVR1* mutations, showing a strong predominance of females in mutant samples. (**d**) Age distribution (left) and overall survival (right) of DIPG cases with *ACVR1* mutations compared to cases with wild-type *ACVR1*. (**e**) Bar plots representing the histological breakdown of samples with mutant and wild-type *ACVR1*. Brown, World Health Organization (WHO) grade 4; orange, WHO grade 3; tan, WHO grade 2. (**f**) Circos plots representing the whole-genome sequences of the four DIPG cases with concurrent *ACVR1* mutation, *HIST1H3B* mutation encoding p.Lys27Met and wild-type *TP53*. The outer ring contains chromosomal ideograms, annotated for somatic SNVs in coding genes. The middle ring plots copy number derived from coverage data: dark red, amplification; pink, gain; dark blue, deletion; light blue, loss. The inner ring represents loss of heterozygosity (LOH; yellow). Drawn inside the circle are structural variations: red, interchromosomal translocation; blue, intrachromosomal translocation; orange, deletion; purple, inversion.

position 328 (c.982G>T, p.Gly328Trp) (**Supplementary Fig. 5**). Overall, we identified 11 of 52 DIPG samples (21%) harboring mutation in *ACVR1* at 4 different codons (**Fig. 2a**). These mutations appear highly specific to DIPG. SNVs in the *ACVR1* coding region are present in the Catalogue of Somatic Mutations in Cancer (COSMIC) database[9] at an overall frequency of 20 in 5,965 (0.3%), with no individual tumor type harboring them with a frequency of greater than 2% and no mutations observed to affect any of the

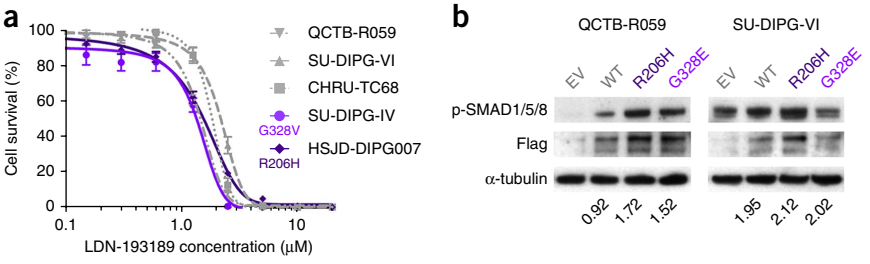

Figure 3 *ACVR1* mutations are weakly activating and responsive to targeted inhibition. (**a**) *In vitro* cytotoxicity of the ALK2 inhibitor LDN-193189. Primary cultures were treated with inhibitor for 72 h, and cell viability was measured by CellTiter-Glo in triplicate experiments. Error bars, s.d. The cells used were HSJD-DIPG007 (DIPG; *ACVR1* Arg206His, *H3F3A* Lys27Met), SU-DIPG-IV (DIPG; *ACVR1* Gly328Val, *HIST1H3B* Lys27Met), CHRU-TC68 (DIPG; *ACVR1* wild type, *H3F3A* Lys27Met), SU-DIPG-VI (DIPG; *ACVR1* wild type, *H3F3A* Lys27Met) and QCTB-R059 (thalamic pediatric GBM; *ACVR1* wild type, *H3F3A* Lys27Met). (**b**) *ACVR1* mutations confer increased signaling through phosphorylated SMAD1/5/8. QCTB-R059 and SU-DIPG-VI cells were transfected with construct encoding Flag-tagged Arg206His or Gly328Glu mutant ALK2 and assessed for phosphorylated SMAD1/5/8 (p-SMAD1/5/8) by protein blot. EV, empty vector; WT, wild-type ALK2. α-tubulin is included as a loading control. Numbers below each lane represent phosphorylated SMAD1/5/8 levels quantified relative to the levels of Flag expression.

residues described in the present study, suggestive of a 'passenger' effect in other cancers.

ACVR1 mutations were found to cosegregate with the less common *HIST1H3B* mutation encoding p.Lys27Met in the canonical histone H3.1 variant ($P < 0.0001$, Fisher's exact test) (**Fig. 2b**), as well as with wild-type *TP53* ($P = 0.0103$, Fisher's exact test). There was also an association between H3.1 alteration and chromosome 2 gain (on which *ACVR1* is found at 2q24.1; $P = 0.0009$, Fisher's exact test). *ACVR1* mutations seem to mark a distinct subset of DIPG cases (**Supplementary Table 2**). There was a marked predominance of females in the *ACVR1*-mutant tumor group compared to cases with wild-type *ACVR1* (1.75:1 versus 0.64:1 female to male ratios, respectively; $P = 0.05$, Fisher's exact test) (**Fig. 2c**), as well as a relatively restricted age of onset (**Fig. 2d**). Cases with tumors harboring *ACVR1* mutations also had longer overall survival times (median of 14.9 versus 10.9 months; $P = 0.05$, log-rank test) (**Fig. 2d**), although outcome remained very poor. There were no significant differences in histology between the groups (**Fig. 2e**). Whole-genome sequencing of biopsy samples exemplifying the genotype with concurrent *ACVR1* and *HIST1H3B* mutations harbored an additional 10–19 somatic SNVs and 0–9 structural variations (**Fig. 2f**).

Remarkably, these somatic mutations in *ACVR1* affected identical residues as the ones described in the germ line of individuals with the autosomal dominant congenital childhood developmental disorder FOP (MIM 135100)[2]. This debilitating disease is characterized by heterotopic ossification of soft connective tissue resulting in severe skeletal abnormalities[10]. Individuals with classical clinical features of FOP carry heterozygous mutations in *ACVR1* encoding p.Arg206His that affect the GS activation domain[11], whereas atypical cases with a less severe phenotype have been shown to harbor either mutations encoding p.Arg258Ser[12], p.Gly328Glu, p.Gly328Arg or p.Gly328Trp[13] or p.Gly356Asp[14] or other heterozygous mutations affecting the GS and kinase domains[2,15]. This latter series of alterations may be exposed to be present at the interface with the GS domain and may abrogate interactions with the negative regulator FKBP12 (refs. 12,13,15). These mutations have been shown to constitutively activate the bone morphogenetic protein (BMP)-dependent transforming growth factor (TGF)-β pathway in the absence of ligand binding, as evidenced by increased phosphorylation of SMAD1, SMAD5 and SMAD8 (SMAD1/5/8) *in vitro*[14,16].

To investigate the specific role of *ACVR1* mutations in the context of DIPG, we assembled a panel of four DIPG case-derived primary cultures (and one thalamic pediatric GBM (glioblastoma multiforme) culture harboring an *H3F3A* mutation encoding p.Lys27Met), representing two *ACVR1* mutations (encoding p.Arg206His and p.Gly328Val) and three wild-type lines (**Supplementary Table 3**). In these models, RNA sequencing (RNA-seq) data demonstrated that the mutant allele was expressed in approximately half of the reads, which was also evidenced by Sanger sequencing of cDNA from case sample NCHP_DIPG011 (**Supplementary Fig. 6**). Treatment with the selective ALK2 inhibitor LDN-193189 (ref. 17) resulted in marked inhibition of cell viability in all cells, with GI_{50} values (concentrations required to inhibit cell growth by 50%) ranging from 0.86–2.1 μM, approximately tenfold lower than with the less potent parent compound dorsomorphin, with a trend toward increased sensitivity in the mutant cultures ($P = 0.10$, F test) (**Fig. 3a**). Transfection of thalamic GBM and DIPG cells with wild-type *ACVR1* (both with *H3F3A* mutation encoding p.Lys27Met) with constructs encoding Flag-tagged mutants conferred increased signaling through phosphorylated SMAD1/5/8, particularly for the Arg206His mutant and, to a lesser extent, for the Gly328Glu mutant (**Fig. 3b**). *ACVR1* mutation may only be one mechanism by which this pathway is activated in DIPG, however, as high basal levels of phosphorylated SMAD1/5/8 were also observed for the cells with *H3F3A* mutation encoding p.Lys27Met and wild-type *ACVR1* that were used in this study (**Supplementary Fig. 7**). This finding may explain the lack of a more robust genotype-dependent response to the inhibitor and may also expand the population of patients who might benefit from targeting of the receptor.

There are no reports to our knowledge of coincident FOP and DIPG, although the clinical features of both typical and atypical cases of FOP can commonly include neurological symptoms and have been reported in children to include cerebellar and brain stem abnormalities[15,18], including demyelinated lesions in the pons, both in human cases and mouse models[19]. It will nonetheless be a challenge to identify the mechanism by which the temporal and spatial context of BMP–TGF-β pathway activation confers such differing clinical phenotypes. In experimental models of FOP, *ACVR1* mutations are associated with defects in stem cell maintenance, reprogramming and differentiation, offering links with cancer-related cellular processes. First-generation ALK2 inhibitors such as dorsomorphin[20] and LDN-193189 (ref. 17) have been shown to downregulate intracellular BMP–TGF-β signaling and to reduce heterotypic ossification, opening the tantalizing possibility of central nervous system (CNS)-penetrant compounds showing a similar potential in a childhood brain tumor otherwise devoid of efficacious treatment options.

URLs. Burrows-Wheeler Aligner (BWA), http://bio-bwa.sourceforge.net/; Picard, http://picard.sourceforge.net/; Genome Analysis Toolkit, http://www.broadinstitute.org/gatk/; SVDetect, http://svdetect.sourceforge.net/; Ensembl Variant Effect Predictor, http://www.ensembl.org/info/docs/variation/vep/; SIFT, http://sift.jcvi.org/; PolyPhen, http://genetics.bwh.harvard.edu/pph2; Catalogue of Somatic Mutations in Cancer (COSMIC) v64, http://www.sanger.ac.uk/genetics/CGP/cosmic/; dbSNP Build 137, http://www.ncbi.nlm.nih.gov/sites/SNP; circular binary segmentation, http://www.bioconductor.org/; APOLLOH, http://compbio.bccrc.ca/software/apolloh/; St. Jude Washington University Protein Paint tool, http://www.explorepcgp.org/; R3.0.1, http://www.r-project.org/.

METHODS

Methods and any associated references are available in the online version of the paper.

Accession codes. Raw data have been submitted to the European Genome-phenome Archive under accession EGAS00001000572.

Note: Any Supplementary Information and Source Data files are available in the online version of the paper.

ACKNOWLEDGMENTS

This study was funded by the Cancer Research UK Genomics Initiative (A14078) and makes use of data generated by the St. Jude Children's Research Hospital–Washington University Pediatric Cancer Genome Project. We are grateful to the DIPG Preclinical Consortium funded by The Cure Starts Now and the Lyla Nsouli Foundation for RNA-seq data. This work is supported by the Stavros Niarchos Foundation, Abbie's Army, the Lyla Nsouli Foundation, the Royal Marsden Hospital Children's Department Fund and Fondo Alicia Pueyo. M.M. gratefully acknowledges funding by the National Institutes of Neurological Disease and Stroke (NINDS; grant K08NS070926), Alex's Lemonade Stand Foundation, the McKenna Claire Foundation and the Dylan Jewett, Elizabeth Stein, Connor Johnson and Zoey Ganesh Memorial Funds. C.P. acknowledges funding from the Agence National de la Recherche. N.T., C.P. and J.G. acknowledge funding from the charity l'Etoile de Martin, and N.E.-W. acknowledges support from Enfants et Santé. A.M.C. acknowledges funding from the Fundación Científica de la Asociación Española Contra el Cáncer. W.J.I. acknowledges funding from the Children's Health Foundation Queensland and the Brainchild Foundation. The Structural Genomics Consortium is a registered charity (1097737) that receives funds from AbbVie, Boehringer Ingelheim, the Canada

Foundation for Innovation, the Canadian Institutes for Health Research, Genome Canada, GlaxoSmithKline, Janssen, Lilly Canada, the Novartis Research Foundation, the Ontario Ministry of Economic Development and Innovation, Pfizer, Takeda and the Wellcome Trust (092809/Z/10/Z). K.R.T., A.M., M.V., D. Carvalho, D.H. and C.J. acknowledge National Health Service (NHS) funding to the National Institute of Health Research Biomedical Research Centres.

AUTHOR CONTRIBUTIONS

C.J., J.G., D.H. and S.Y. designed the study. C.J. wrote the manuscript. K.R.T., A.M. and C.J. designed and reviewed experiments, and designed and reviewed statistical and bioinformatic analyses. K.R.T. performed experiments. A.M. performed bioinformatic analyses. N.T., D. Castel, M.V. and D. Carvalho performed sample preparation and experiments. Y.S.B., O.M., C.P., C.S.G. and S.Y. performed and reviewed bioinformatic analyses. A.M.C., C.d.T., O.C., J.M., N.E.-W., W.J.I., M.M., A.N.B., S.P. and J.G. provided and prepared samples and experimental materials. All authors reviewed the manuscript during its preparation.

COMPETING FINANCIAL INTERESTS

The authors declare no competing financial interests.

1. Jones, C., Perryman, L. & Hargrave, D. Paediatric and adult malignant glioma: close relatives or distant cousins? *Nat. Rev. Clin. Oncol.* **9**, 400–413 (2012).
2. Katagiri, T. Recent topics in fibrodysplasia ossificans progressiva. *J. Oral Biosciences* **54**, 119–123 (2012).
3. Wu, G. *et al.* Somatic histone H3 alterations in pediatric diffuse intrinsic pontine gliomas and non-brainstem glioblastomas. *Nat. Genet.* **44**, 251–253 (2012).
4. Lewis, P.W. *et al.* Inhibition of PRC2 activity by a gain-of-function H3 H3 mutation found in pediatric glioblastoma. *Science* **340**, 857–861 (2013).
5. Roujeau, T. *et al.* Stereotactic biopsy of diffuse pontine lesions in children. *J. Neurosurg.* **107**, 1–4 (2007).
6. Schwartzentruber, J. *et al.* Driver mutations in histone H3.3 and chromatin remodelling genes in paediatric glioblastoma. *Nature* **482**, 226–231 (2012).
7. Puget, S. *et al.* Mesenchymal transition and *PDGFRA* amplification/mutation are key distinct oncogenic events in pediatric diffuse intrinsic pontine gliomas. *PLoS ONE* **7**, e30313 (2012).
8. Paugh, B.S. *et al.* Genome-wide analyses identify recurrent amplifications of receptor tyrosine kinases and cell-cycle regulatory genes in diffuse intrinsic pontine glioma. *J. Clin. Oncol.* **29**, 3999–4006 (2011).
9. Forbes, S.A. *et al.* COSMIC: mining complete cancer genomes in the Catalogue of Somatic Mutations in Cancer. *Nucleic Acids Res.* **39**, D945–D950 (2011).
10. Shore, E.M. & Kaplan, F.S. Inherited human diseases of heterotopic bone formation. *Nat. Rev. Rheumatol.* **6**, 518–527 (2010).
11. Shore, E.M. *et al.* A recurrent mutation in the BMP type I receptor *ACVR1* causes inherited and sporadic fibrodysplasia ossificans progressiva. *Nat. Genet.* **38**, 525–527 (2006).
12. Bocciardi, R., Bordo, D., Di Duca, M., Di Rocco, M. & Ravazzolo, R. Mutational analysis of the *ACVR1* gene in Italian patients affected with fibrodysplasia ossificans progressiva: confirmations and advancements. *Eur. J. Hum. Genet.* **17**, 311–318 (2009).
13. Petrie, K.A. *et al.* Novel mutations in *ACVR1* result in atypical features in two fibrodysplasia ossificans progressiva patients. *PLoS ONE* **4**, e5005 (2009).
14. Fukuda, T. *et al.* A unique mutation of ALK2, G356D, found in a patient with fibrodysplasia ossificans progressiva is a moderately activated BMP type I receptor. *Biochem. Biophys. Res. Commun.* **377**, 905–909 (2008).
15. Kaplan, F.S. *et al.* Classic and atypical fibrodysplasia ossificans progressiva (FOP) phenotypes are caused by mutations in the bone morphogenetic protein (BMP) type I receptor ACVR1. *Hum. Mutat.* **30**, 379–390 (2009).
16. Chaikuad, A. *et al.* Structure of the bone morphogenetic protein receptor ALK2 and implications for fibrodysplasia ossificans progressiva. *J. Biol. Chem.* **287**, 36990–36998 (2012).
17. Yu, P.B. *et al.* BMP type I receptor inhibition reduces heterotopic ossification. *Nat. Med.* **14**, 1363–1369 (2008).
18. Tumolo, M., Moscatelli, A. & Silvestri, G. Anaesthetic management of a child with fibrodysplasia ossificans progressiva. *Br. J. Anaesth.* **97**, 701–703 (2006).
19. Kan, L. *et al.* CNS demyelination in fibrodysplasia ossificans progressiva. *J. Neurol.* **259**, 2644–2655 (2012).
20. Yu, P.B. *et al.* Dorsomorphin inhibits BMP signals required for embryogenesis and iron metabolism. *Nat. Chem. Biol.* **4**, 33–41 (2008).

ONLINE METHODS

Tumor cohort. DIPG samples and matched peripheral blood samples were available from 21 patients who underwent stereotactic biopsy at the Neurosurgery Department of Necker Sick Children's Hospital (Paris, France), 20 of which were subjected to whole-genome sequencing. All patients were clinically diagnosed as having DIPG on the basis of clinical presentation and radiography as part of a multidisciplinary assessment. These patients had diffuse intrinsic tumor centered in the pons and occupying at least 50% of the volume of this structure and had an associated short clinical history of less than 3 months. DNA from an additional 26 biopsy samples was available as a validation cohort. A further five DIPG cases with matched peripheral blood samples were obtained at autopsy at the Hospital Sant Joan de Déu (Barcelona, Spain) and were sequenced after exome capture using Agilent SureSelect technology. All patient material was collected after informed consent and was subject to local research ethics committee approval. Cases included 23 girls and 29 boys (1:1.26 ratio). The median age of the patients was 6.6 years, and the median overall survival time was 11.6 months. A summary of the tumor cohort and clinicopathological information are provided in **Supplementary Table 2**.

Whole-genome and whole-exome sequencing. Exome capture was carried out on the four autopsy cases using the 50Mb Agilent SureSelect platform (Agilent Technologies), and samples underwent paired-end sequencing on an Illumina HiSeq 2000 with a 100-bp read length. Library preparation for the biopsy samples was carried out by the Illumina FastTrack service, and entire genomes underwent paired-end sequencing on an Illumina HiSeq 2000. The median coverage for the tumor genomes was 37–67× (matched normal genomes, 34–41×). Reads were mapped to the hg19 build of the human genome using BWA (Burrows-Wheeler Aligner), and PCR duplicates were removed with PicardTools 1.5.

Genome analysis. Somatic SNVs were called using the Illumina Genome Network (IGN) Cancer Normal pipeline version 1.0.2 and the Genome Analysis Toolkit v2.4-9. Structural variations were called using IGN and SVDetect. Variants were annotated using the Ensembl Variant Effect Predictor v71 tool incorporating SIFT and PolyPhen predictions, COSMIC v64 and dbSNP Build 137 annotations. Copy number was obtained by calculating $\log_2$ ratios of tumor/normal coverage binned into exons of known genes, smoothed using circular binary segmentation and processed using in-house scripts. LOH was calculated using APOLLOH. Schematics showing the locations of recurrent mutations were produced by the St. Jude Washington University Protein Paint tool. Statistical analysis was carried out using R3.0.1. Continuous variables were analyzed using Student's *t* tests. Count data were compared using Fisher's exact test.

Cell culture and drug sensitivity. Primary cultures were derived from DIPG case samples taken at either biopsy or autopsy at multiple centers, representing both cases with mutant and wild-type *ACVR1* and with both *H3F3A* and *HIST1H3B* mutations encoding p.Lys27Met, in addition to cells from a pediatric glioblastoma specimen arising in the thalamus with an *H3F3A* mutation encoding p.Lys27Met. A summary of the cases from which these cells were derived is provided in **Supplementary Table 3**. Cells were grown under adherent stem cell conditions using flasks coated with laminin (Sigma) in neurobasal medium (Invitrogen) supplemented with B-27 (Invitrogen) and the growth factors epidermal growth factor (EGF), basal fibroblast growth factor (bFGF), platelet-derived growth factor (PDGF)-AA and PDGF-BB (all from Shenandoah Biotech). The ALK2 inhibitors LDN-193189 (Sigma) and dorsomorphin (Abcam) were tested for their effects on cell viability using a highly sensitive luminescent assay measuring cellular ATP levels (CellTiter-Glo, Promega). Drug was added in various concentrations, and cells were assayed in triplicate after 72 h. Statistical analysis was carried out using GraphPad Prism 6.0 (GraphPad Software).

Allelic expression of *ACVR1*. SU-DIPG-IV cells were subjected to full transcriptome sequencing as part of the DIPG Preclinical Consortium. Counts of reads aligned to the *ACVR1* coding region in NCBI_36 were analyzed for the ratio of mutant to wild-type sequence and visualized in Genome Browse (Golden Helix). RNA from the NCHP_DIPG011 primary tumor was reverse transcribed, PCR amplified and underwent Sanger sequencing to determine whether both mutant and wild-type alleles were expressed (**Supplementary Table 4**).

Overexpression of mutant ALK2. The *ACVR1* mutations encoding p.Arg206His and p.Gly328Glu were introduced into pcDNA3.1 by site-directed mutagenesis as previously described[16], and constructs were transfected into primary QCTB-R059 and SU-DIPG-VI cells using Lipofectamine (Invitrogen), with protein collected after 24 h using standard procedures. Protein blotting was carried out with horseradish peroxidase (HRP)-conjugated antibody to Flag (A8592, Sigma; 1:1,000 dilution) and antibody to phosphorylated SMAD1/5/8 (9511, Cell Signaling Technology; 1:1,000 dilution) under standard conditions. Relative levels of phosphorylated SMAD1/5/8 were measured with ImageJ software (National Institute of Mental Health).

Statistical analysis. Statistical analysis was carried out using GraphPad Prism 6.0 and R 3.0.1. Comparisons of the numbers of coding SNVs and the mutation rates in biopsy and autopsy cases were performed by *t* test. For analysis of categorical association between cases with *ACVR1* mutations and mutations in *HIST1H3B* or *TP53*, sex and histology, Fisher's exact test was used. Differences in survival were analyzed by the Kaplan-Meier method, and significance was determined by the log-rank test. All tests were two-sided, and a *P* value of less than 0.05 was considered significant. A sum-of-squares F test was used to assess differences in dose response curves for *ACVR1*-mutant versus wild-type cells.

doi:10.1038/ng.2925